Charge ordering and long-range interactions in layered transition metal oxides: A quasiclassical continuum study

Branko P. Stojković,[1] Z. G. Yu,[2] A. L. Chernyshev,[3,*] A. R. Bishop,[1] A. H. Castro Neto,[3] and Niels Grønbech-Jensen[4]
[1]*Theoretical Division and Center for Nonlinear Studies, Los Alamos National Laboratory, Los Alamos, New Mexico 87545*
[2]*Department of Chemistry, Iowa State University, Ames, Iowa 50011*
[3]*Department of Physics, University of California, Riverside, California 92521*
[4]*Department of Applied Science, University of California, Davis, California 95616*
and NERSC, Lawrence Berkeley Laboratory, Berkeley, California 94720
(Received 24 November 1999)

The competition between long-range and short-range interactions among holes moving in an antiferromagnet (AF) is studied within a model derived from the spin-density-wave picture of layered transition metal oxides.A novel numerical approach is developed that allows one to solve the problem at finite hole densities in very large systems (of the order of hundreds of lattice spacings), albeit in a quasiclassical limit, and to correctly incorporate the long-range part of the Coulomb interaction. The focus is on the problem of charge ordering and the charge phase diagram: at low temperatures four different phases are found, depending on the strength of the magnetic (dipolar) interaction generated by the spin-wave exchange and the density of holes. The four phases are the Wigner crystal, diagonal stripes, a grid phase (horizontal-vertical stripe loops), and a glassy-clumped phase. In the presence of both in-plane and out-of-plane charged impurities the stripe ordering is suppressed, although finite stripe segments persist. At finite temperatures multiscale (intermittency) dynamics is found, reminiscent of that in glasses. The dynamics of stripe melting and its implications for experiments is discussed.

I. INTRODUCTION

Charge ordering in layered transition metal oxides has recently attracted significant research interest, due to its possible relation to the mechanism of high-temperature superconductivity in doped cuprates[1] and bismuthates.[2] In particular, stripelike ordering, which involves holes ordered into linear arrays, separated by an antiferromagnetically (AF) ordered electronic background, has discussed as a candidate for the explanation of pseudogap effects in underdoped cuprate compounds.[1] In addition, the formation of domain walls has been discussed in terms of the proximity to phase separation.[3] Quite generally, phase separation on mesoscopic and even macroscopic scales is potentially relevant for any strongly correlated organic and inorganic electronic system, including systems with spin-density-wave (SDW),[4] charge-density-wave (CDW),[5] and Jahn-Teller broken-symmetry[6] ground states.

On the experimental side, mesoscopic (nanoscale) phase separation has been observed in many compounds. In the case of $La_{2-x}Sr_xNiO_{4+y}$ stripes have been observed both using nuclear magnetic resonance (NMR) methods and more directly, using high-resolution electron diffraction.[7] In addition, stripes have also been identified in $La_{1-x}Ca_xMnO_3$ for specific commensurate values of doping.[8] In cuprates static stripe order has been observed in $La_{1.6-x}Sr_xNd_{0.4}CuO_4$ in both elastic and inelastic neutron scattering experiments,[9] and *x*-ray diffraction experiments.[10] There are also evidences that stripes exist in some form in high-T_c compounds. In the oxygen-doped $La_2CuO_{4+\delta}$ (Ref. 11) stripes have been observed using nuclear magnetic resonance (NMR) techniques. Magnetic susceptibility measurements,[12] nuclear quadrupole resonance[13] (NQR), and muon spin resonance[14] all indicate formation of domains in $La_{2-x}Sr_xCuO_4$. Recent inelastic neutron scattering (INS) experiments in $La_{2-x}Sr_xCuO_4$ and $YBa_2Cu_3O_{7-\delta}$, (YBCO) superconductors yield results consistent with stripe formation,[15–17] although the width of the INS lines in, e.g., YBCO materials is large, which may suggest dynamic charge ordering.

On the theoretical side, stripes have been proposed by several research groups. In strongly correlated systems, such as cuprate superconductors, electrons exhibit a strong on-site repulsion. Therefore numerous studes have been devoted to the Hubbard and *t-J* models. It has been shown that a mean-field treatment of the Hubbard model yields a stripe phase as a locally stable solution.[18] Many other studies view the stripes as an outcome of the competition between kinetic energy of holes and exchange energy of spins alone and frequently neglect the role of the long-range part of the Coulomb interaction.[19,20] Only recently has an attempt to incorporate the long-range forces into the mean-field approach to the Hubbard model been made.[21] Another point of view emphasizes the intrinsic instability of a strongly correlated electronic system towards a phase separation as a necessary starting point.[22,23] Then it is assumed that such an instability is prevented by the long-range Coulomb forces. Therefore, the competition between this instability, whose existence in the physical range of parameters of the realistic models is yet to be proven, and Coulomb repulsion gives rise to a stripe phase. Thus, these two approaches agree on the importance of the correlations but disagree on the role of long-range forces. More recently, it has been shown that phase separation is indeed a very common phenomenon close to quantum critical points.[24]

One would expect that the existence of stripes in the widely studied ''minimal'' t-J or Hubbard models can be either proven or disproven by some unbiased numerical technique. Unfortunately, numerically the stability of the stripe phase has been established less clearly. Numerical studies of the t-J model present conflicting conclusions as to the existence of stripe phases in the ground state of this ''basic'' strongly correlated model, which might be the result of the strong finite-size effects.[25,26] For example, even a Monte Carlo simulation of the doped Ising model, without the long-range forces, yields holes ordered into loops, rather than into geometric arrays.[27] In fact, with the exception of the recent density matrix renormalization group (DMRG) simulations of White and Scalapino,[25] which have found stripe formation in relatively large t-J clusters, no microscopic calculation to date has shown that the stripes are a stable entity. Most importantly, no stripe formation in a system with long-range interaction has been studied in a direct simulation. In addition, the sizes of the clusters available with modern day computers for solving quantum models of spins and holes are still too small to study role of the the long-range Coulomb interaction and be free from significant finite-size effects.

In this situation we propose a different strategy: one can study a quasiclassical limit of the quantum problem of holes in an AF spin environment analytically and incorporate all essential correlations in an effective hole-hole interaction. In this case the AF background is effectively integrated out, and the focus is on the charge subsystem. Then the motion of ''classical'' holes at finite density, interacting via an *effective* magnetic interaction and in the presence of long-range Coulomb forces, can be studied numerically in much larger systems. In other words, in this paper we combine analytical and numerical approaches to study the charge ordering in transition metal oxides.

Our numerical approach is based on the SDW picture of Schrieffer, Wen, and Zhang,[28] which is closely related[29] to the semiclassical approach to the t-J model by Shraiman and Siggia[30] in which the interaction between doped holes stems from the spiral distortion of the local Néel vector near a hole. As shown below, in the quasiclassical limit, the problem can be solved using classical Monte Carlo (MC) or molecular dynamics (MD) methods. In a systematic numerical study we explore the interplay between long-range Coulomb interaction and short (or intermediate)-range AF interactions of dipolar nature, which we take to have both isotropic and anisotropic components (depending on the lattice structure).

Our main results can be summarized as follows: in the absence of disorder we find four phases depending on the density of holes and the characteristic AF energy scales: (i) a Wigner crystal, (ii) diagonal (glassy) stripes, (iii) a geometric phase, characterized by horizontal-vertical stripes or a checkerboard (grid), and (iv) a ''clumped'' phase (phase separation). In our study the stripelike phases emerge as a kind of melting of the Wigner crystal phase; hence the long-range Coulomb interaction is a necessary ingredient for their occurrence. In the geometric phase the stripes, resulting from the competition of the short-range and long-range interactions, are characterized by a particular AF dipolar alignment. The patterns are very stable, showing large ''string tension,'' while the motion of holes within a stripe is much softer. If one takes into account the kinetic energy of the holes along the stripes one is lead to the concept of a quantum liquid crystal as proposed recently by Kivelson, Fradkin, and Emery.[31] On the other hand, the ground state of the geometric phase is not well defined in that there are many geometric phases with very low energies, comparable to that of the ground state, implying a *rugged energy landscape*. We find that on lowering the temperature, the geometric hole ordering is characterized by the occurence of secondary defects in the structure. At higher temperatures we find that the *dynamic* hole ordering is characterized by *temporally intermittent* pattern formation (i.e., spatiotemporal intermittency). Finally, we find that a sufficient concentration of randomly placed impurities destroys the geometric hole pattern, although, regardless of the impurity type, stripe *segments* are preserved.

The paper is organized as follows: in the next section we present a review of the theoretical model and the computational methods we use. In Sec. III we present our numerical results and in particular we present the phase diagram showing how the obtained phases emerge as a function of doping and interaction strengths. Finally, in Sec. IV we summarize our conclusions and experimental implications.

II. MODEL

We begin with the SDW picture of layered transition metal oxides. This picture has been very successful in describing the stoichiometric insulating AF phase of these systems at low temperatures.[32,28] In this picture the electrons move with hopping energy t in the self-consistent staggered field of its spin, as described by, e.g., the Hubbard model (the calculation is presented in detail in Appendix A):

$$H=-t\sum_{\langle i,j\rangle}(c_i^{\dagger}c_j+\text{H.c.})+U\sum_i n_{i,\uparrow}n_{i,\downarrow}. \tag{1}$$

Because the translational symmetry of the system is broken, the electronic band is split into upper and lower Hubbard bands.[33] On performing a Bogoliubov transformation, one defines the valence ($h_{k,\alpha}$) and conduction band ($p_{k,\alpha}$) operators, respectively:

$$p_{k,\alpha}=u_k c_{k,\alpha}+\alpha v_k c_{k+Q,\alpha}, \tag{2}$$

$$h_{k,\alpha}=u_k c_{k,\alpha}-\alpha v_k c_{k+Q,\alpha}, \tag{3}$$

where u_k, v_k are the Bogolioubov weights and α is the sublattice index. The upper and lower Hubbard bands are separated by the Mott-Hubbard gap, $\Delta=US/2$, where S is the expectation value of the staggered field S_z,

$$\langle S_z(\mathbf{q})\rangle=-2\sum_{k,\alpha}u_{k+q-Q}v_k\langle h_{k+q-Q,\alpha}h_{k,\alpha}^{\dagger}\rangle, \tag{4}$$

calculated at momentum transfer $\mathbf{q}=\mathbf{Q}$. At half filling the lower band is filled and the upper band is empty. This picture is consistent with the angle-resolved photoemission data in the layered AF insulator $Sr_2CuO_2Cl_2$.[34] On doping the system with holes with planar density σ_s, at low temperatures, $T\ll\Delta/k_B$, the low-frequency physics reflects purely the lower Hubbard band (LHB). It has been shown[35] that, regardless of the band structure, the LHB has a maximum at four wave vectors $\mathbf{k}_i=(\pm1,\pm1)\pi/(2a)$, where a is the lat-

tice spacing, and therefore the long-wavelength theory of the problem can be studied by assuming the momentum of the holes to be close to these points.

Then the two-hole interaction Hamiltonian can be separated into the longitudinal and transverse parts (H_z and H_{xy}, respectively), whose Fourier transform, for quasiparticle momenta near k_i, is equal to[29]

$$H(\mathbf{r})=[A_z\sigma_1^z\sigma_2^z-A_{xy}(\sigma_1^+\sigma_2^-+\sigma_1^-\sigma_2^+)]\delta(\mathbf{r}) -B_{xy}\left[\frac{\mathbf{d}_1\cdot\mathbf{d}_2}{r^2}-2\frac{(\mathbf{d}_1\cdot\mathbf{r})(\mathbf{d}_2\cdot\mathbf{r})}{r^4}\right](\sigma_1^+\sigma_2^-+\sigma_1^-\sigma_2^+), \tag{5}$$

where $r=|\mathbf{r}_1-\mathbf{r}_2|$ is a relative hole-hole distance, $\mathbf{r}_i$ is a coordinate of a hole in units of a, $\sigma_i^{z(\pm)}=c_\alpha^\dagger\sigma_{\alpha\beta}^{z(\pm)}c_\beta$ is a spin-density operator, with $\sigma^{z(\pm)}$ Pauli matrices, and $\mathbf{d}_i$ is a unit vector in the direction of the dipole moment of the hole. In the SDW formalism the interaction strengths A_z, A_{xy}, and $B_{xy}\sim A_{xy}/2\pi$ are all of order Hubbard U. The interaction (5) is clearly rotationally invariant and valid for $r\geqslant a$, while for $r\to 0$ it yields an unphysical divergence of the (attractive) dipolar interaction. We observe that this form of the Hamiltonian is not particular to the SDW theory of the Hubbard model, but stresses the fact that a mobile carrier in an antiferromagnet produces a dipolar distortion of the magnetic background. We demonstrate this explicitly in Appendix B where we show that the t-J model has exactly the same type of interaction terms. In other words, at finite density the holes interact via two different mechanisms: a uniform short-range attractive force due to AF bond breaking and a long-range magnetic dipolar interaction [contained by Eq. (5), see Ref. 28]. The latter term is due to the long-range spiral distortion of the AF background, which is a consequence of quasiparticles interacting with soft (Goldstone) modes of the spin system.[29,30] The magnetic dipole moment associated with each hole is due to the coherent hopping of holes between different sublattices and scales with the AF magnetic energy. This implies that the quantum effects associated with hole kinetic energy can be neglected, which is correct in the limit $t\ll J$, believed to be valid in nickelates. This is also why the hole-hole interaction obtained in the weak coupling SDW picture is equivalent[29] to that in the effective Hamiltonian found by Shraiman and Siggia,[30] based on the t-J model, where the *dipolar* interaction is obtained using *semiclassical* analysis of the spin part of the model, as well as symmetry considerations. It is also possible to prove, using Ward identities, that the remaining spin part of the problem is equivalent to the two-dimensional (2D) nonlinear σ model in the long-wavelength limit.[36] It has been argued[30] that at physical values $t/J\gg 1$ all coupling strengths (A_z, A_{xy}, and B_{xy}), and therefore the hole-hole interaction, will be renormalized to the value of superexchange constant J.

In pure two dimensions at finite T the system is magnetically disordered, characterized by a finite magnetic correlation length ξ (see Ref. 37), and the range of the dipolar interaction between the holes, mediated by the AF background, is also of order ξ. In fact, even at $T=0$ and *finite* hole concentration the correlation length is restricted and the dipolar interaction is effectively short ranged.

It has been noted[38] that the dipolar twist of the magnetic background would imply local time-reversal symmetry breaking, which puts some restrictions on the applicability of the picture to the real systems where such symmetry breaking has not been experimentally observed. Indeed, the time-reversal symmetry is already broken in the Néel state, as well as in any magnetically ordered state. However, in two-dimensional spin systems at finite temperature all symmetries are restored and we expect this to be true also for the hole-doped case studied here.

Besides the AF interactions the holes also experience the long-range Coulomb interaction. This is clear if we consider that $r_s=r_0/a_0$ (where r_0 is the mean interparticle distance and a_0 is the Bohr radius) is very large in the underdoped systems ($r_s\approx 8$). In other words, in systems with a small density of holes, the screening, which is due to the density fluctuations, is very weak and one must take the Coulomb interaction into account.

Finally, each hole carries a spin degree of freedom as well. However inspection of Eq. (5) reveals that the overall spin energy is minimized in the spin-antisymmetric channel. Hence we neglect the spin-symmetric channel and thus in our approach, we only consider the charge channel with an effective (magnetic in origin) interaction between two holes, 1 and 2, of the form [see Eq. (5)]

$$V(\mathbf{r})=\frac{q^2}{\epsilon r}-Ae^{-r/a}-B\cos(2\theta-\phi_1-\phi_2)e^{-r/\xi}, \tag{6}$$

where we have asssumed that $\mathbf{r}$ can be relaxed from a crystal lattice position to an arbitrary (continuous) value. We return to this point later.

In Eq. (6) q is the hole charge, ϵ is the dielectric constant (which we assume to be of order 1), θ is the angle made between $\mathbf{r}$ and a fixed axis, and $\phi_{1,2}$ are the angles of the magnetic dipoles relative to the same fixed axis. A is the strength of the uniform (short-range) interaction and B is the strength of the magnetic dipolar interaction, which we will assume to be independent adjustable parameters, which, in real materials, should be of order ~ 1 eV. Note that we have introduced $B\sim B_{xy}/l^2$, where l is some appropriate average length, $a<l<\xi$, in order to avoid the unphysical divergence of the dipolar part of the interaction in Eq. (5), while keeping the necessary symmetry of the interaction. Moreover, in the SDW picture, at low doping, ϕ_1 and ϕ_2 are restricted to the angles $(2n+1)\pi/4$, the four angles determined by the vectors $\mathbf{k}_i$. In addition, the dipole moment vectors are also restricted to $\mathbf{k}_i$, which justifies our use of Eq. (6) where we have assumed a fixed *size* of the dipole moment for each hole. However, at larger doping levels these angles can be relaxed to arbitrary values, provided the interaction is short-ranged. Of course, we have verified by an explicit calculation that restricting dipole angles to the discrete values does not qualitatively change our results, presented in the next section. It is interesting to note that the hole-hole interaction in the form almost identical to Eq. (6) has been obtained by Aharony *et al.*[39] for the *static* holes residing on Cu-O bonds within the framework of a *classical* model of an AF diluted by ferromagnetic bonds. In this case the value of the coupling constant B is also restricted by a few J. Indeed, starting from the insulating phase of cuprates, the holes are injected

into the CuO_2 planes at high temperatures during the sample preparation. The hole distribution in this case is annealed (instead of quenched as proposed in Ref. 39) since the holes have enough phase space for interactions. As the temperature is lowered the holes can adjust themselves to $V(\mathbf{r})$ and form the structures we discuss below.

Quite generally, one can think of an AF as an active media generating long-range dipolar forces in response on some local distortion. Therefore, the interaction $V(\mathbf{r})$, Eq. (6), is of more general significance than just a result of the SDW picture, and the study of the system of particles interacting via $V(\mathbf{r})$ is of wider interest.

In general, the many-body problem of holes in an AF background is extremely complicated, involving many-particle interaction terms. However, at low densities, where the average distance between holes is comparable to the AF correlation length, it is reasonable to assume that the interaction of any two holes is weakly perturbed by other holes, and the total potential energy can be expressed in terms of two-particle energies, provided the AF correlation length is replaced by an *effective* correlation length, which, to avoid clutter, we also denote as ξ. We therefore study the system of ''classical'' particles in a computational box of size $L_x \times L_y$, interacting via a potential

$$H_I = \sum_{\langle i,j \rangle} V(\mathbf{r}_{ij}), \tag{7}$$

where $V(\mathbf{r})$ is given by Eq. (6). However, we emphasize that our approach is not a self-consistent one in the sense that the true interaction must include many-particle terms (omitted here), which stem from the fact that the SDW state is altered due to the charge ordering. The self-consistent approach to charge ordering will be presented elsewhere. In addition, superconducting fluctuations have been neglected. Moreover, the kinetic energy of the holes may lead to a quantum melting of the phases discussed here.

The long-range character of the Coulomb interaction requires further consideration: in order to perform calculations at finite density, as required by the dipolar interaction we consider, we usually perform calculations with periodic boundary conditions. The ability to handle long-range Coulomb interactions in rectangular periodic media has been enhanced recently in the area of molecular physics.[40] Assuming a computational cell of arbitrary geometry and cyclic boundary conditions it is possible to sum interactions of particles with all of their images residing in cells obtained by translation from the original computational cell,[41,40] yielding an effective interaction that is periodic in the computational cell used (see Fig. 1). On making integral transformations, Coulomb interactions are computed by summing over fast-convergent Bessel functions with great accuracy (see Ref. 40 for a detailed study of the Lekner summation technique). The computational efficiency is further enhanced by tabulating the effective interaction. This is possible since the difference between the obtained effective interaction and the Coulomb interaction is a well-behaved function that can be easily calculated using polynomial interpolation.

At the beginning of each simulation we place the holes at random and assign to each hole a magnetic dipole moment of constant size, but random direction. We study the energy

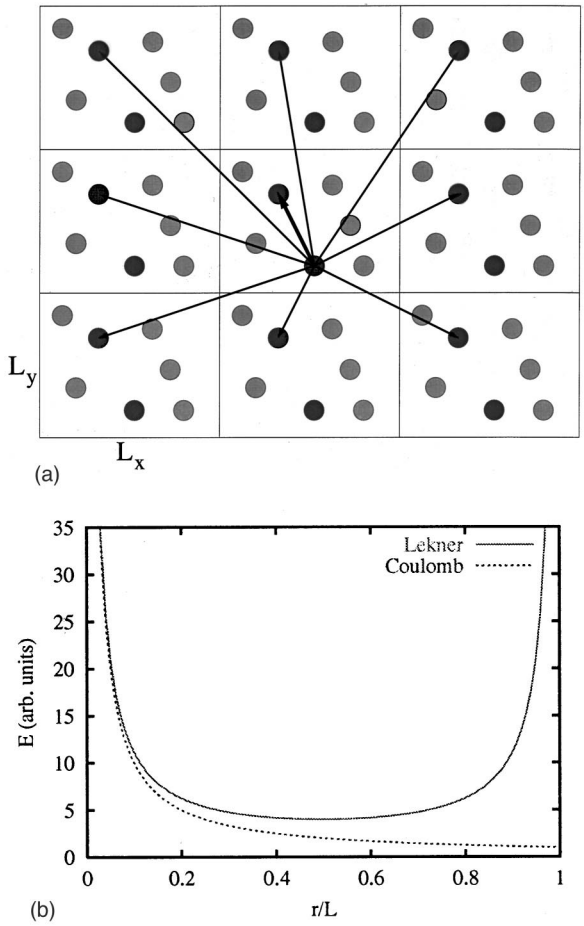

FIG. 1. (a) Electrostatic interaction in a system with periodic boundary condition. An effective interaction between any two charged particles in the computational box (central rectangle), such as the two marked by a thick vector line, involves the interaction with all of the particle images, marked by thin wave vector lines. (b) the Lekner potential (which accounts for the periodic boundary conditions) in comparison with the bare Coulomb potential, within a computational box of size L. As expected, at $r \to 0$ the two potentials coincide (up to an additive constant) and hence their difference can be readily approximated by a low order polynomial.

landscape and the dynamics of the system using three different methods: Monte Carlo (MC), Langevin molecular dynamics (MD), and a hybrid MC-MD method.[42] All three methods yield essentially the same results. Both MC and MD methods are well known in the literature[43] and hence we only review details pertinent to our calculation. In the MC method we use the standard Metropolis algorithm for the acceptance of hole configurations. For the Langevin MD method the dynamics of the system is determined by the forces, obtained from Eq. (7), with a noise term, η_i, for each particle that satisfies the usual fluctuation-dissipation condition $\langle \eta_i \eta_j \rangle = 2\pi\gamma T \delta_{i,j}$, where i,j correspond to all possible degrees of freedom and γ is a damping term.[43] Since the system exhibits several phases (see Fig. 5) for some values of the input parameters, its ground state is not always well defined and a numerically obtained low-temperature state may, in fact, depend on the initial and boundary conditions. Hence, in order to rapidly reach a hole configuration with the lowest global minimum energy, we perform simulated annealing from high temperatures.

The hybrid MC method includes elements of both the MC and MD methods: the hole configuration is again determined using the standard Metropolis algorithm, but here a new configuration is obtained by letting the system evolve through a classical MD calculation over a certain time period. Note that, in principle, in classical MD calculations the energy is a conserved quantity; hence every step should in principle be accepted. In reality the MD method introduces errors which typically slightly lower the system energy, just as required by the Metropolis algorithm. Hence this method yields extremely high MC acceptance ratios.[42]

III. RESULTS

In this section we discuss the results of our numerical calculations. We first present the obtained ordered phases and the phase diagram of the system and discuss its implications. We then show the hole ordering in the presence of disorder. Finally we show the properties of the system as a function of T and in particular the dynamics of the observed (stripe) pattern formation.

Before we begin with the presentation of our results we address the input parameters of the model, namely the hole density, σ_s (or the doping level n), the strengths of the isotropic and dipolar parts of the AF interaction, A and B, respectively, the AF correlation length ξ, the temperature T, and the concentration of impurities, c_i, for the systems with static point disorder. We define the doping level n as the hole density measured in units of the cuprate lattice spacing; thus $n=1\%$ corresponds to 1 hole per $100a^2$, where $a\approx 3.8$ Å.

The input parameters are not necessarily independent of each other, e.g., A and B should be proportional to each other, with $A\approx U$ when $t\gg U$ and $A\approx 4t^2/U$ when $U\gg t$ (see Ref. 29). However, since the range of the bond breaking and dipolar interactions is vastly different, it is reasonable to treat A,B, and ξ as independent parameters. Clearly both A and B should be of order of the Hubbard U in the SDW approach and of the order of J in the strong coupling limit, and the correlation length is of the order of 1 to 10 lattice spacings in cuprates.

We begin with the low-temperature properties (ground state) of the system as a function of B. The relevant order parameter for charge ordering is the Fourier transform of the hole density:

$$\rho(\mathbf{q})=\frac{1}{N}\sum_{i=1}^{N} e^{i\mathbf{q}\cdot\mathbf{r}_i}, \tag{8}$$

where $\mathbf{r}_i$ is the position of the ith hole and N is the total number of holes. A peak in $\rho(\mathbf{q})$ at some wave vector $\mathbf{q}=\mathbf{K}$ indicates ordering. Returning to the SDW picture, presented in Sec. II, we recall that the hole density is given by

$$\rho_k=\sum_{q,\alpha} h^{\dagger}_{k+q,\alpha}h_{q,\alpha}. \tag{9}$$

From the definition of the staggered magnetization, Eq. (4), it is immediately clear that $\langle S_z(q)\rangle\propto\delta_{q,K+Q}$, i.e., a peak in ρ_k at K leads to a magnetic peak at $Q+K$ and by symmetry at $Q-K$.

Since the interaction due to the second term in Eq. (6) (isotropic attractive interaction) is extremely short-range (in fact in an infinite system it is a δ function), it is initially reasonable to set $A=0$ and explore the behavior of the system as a function of B. We return later to the role of A. As explained in Sec. II low-T properties have been obtained by annealing the system from some high temperature ($T\sim 5000$ K) down to temperatures of order 1 K. In the extreme case $B=0$ we find a Wigner crystal with small distortions, to be the state of lowest energy, as expected[44] [see Fig. 2(a)].

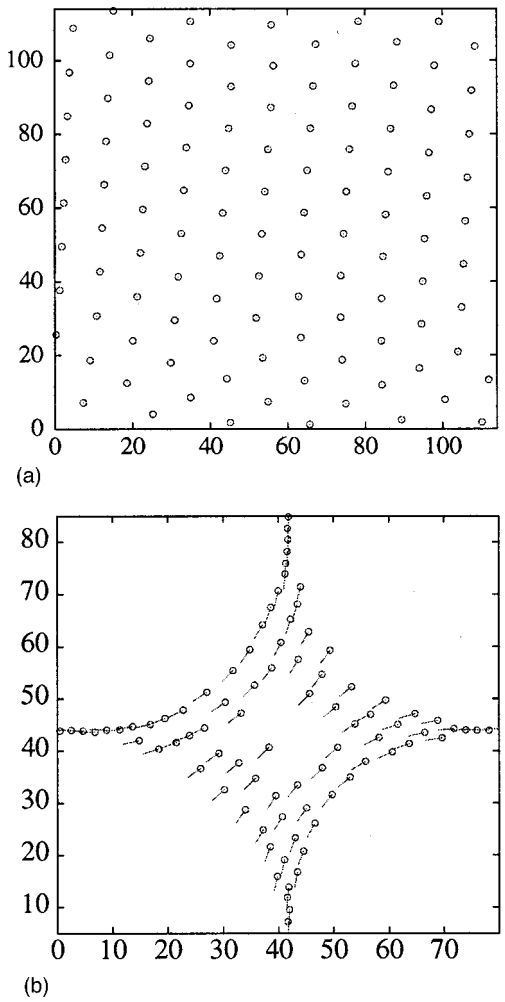

FIG. 2. Low-T states of the hole-vacancy system. (a) For $B=0$ the holes (circles) form the Wigner crystal and (b) for $B\to\infty$ (an unphysical case) they form a ''clump'' pattern, a characteristic of the ''mesoscopic phase separation.'' The dipole orientation (shown by the segments, originating from the circle centers) indicates finite magnetization at each star cluster. In both panels the doping level is $n=15\%$.

The small distortion of the Wigner crystal structure is due to the periodicity, which introduces a small spatial anisotropy into the system due to the shape of the computational box. Indeed, upon setting, e.g., $L_y/L_x=\sqrt{3}/2$, we obtain a perfect Wigner crystal to be the ground state. Another extreme case is when $B\to\infty$. In this case the AF dipolar interaction dominates over the average Coulomb interaction; one then finds star-shaped clumps of holes, similar in shape to those found in Ref. 45, which can, at sufficiently high density, form a geometric structure (e.g., a Wigner crystal of clumps). We note that this case is rather unphysical, as macroscopic phase separation is inconsistent with our initial as-

sumption of the two-body dipolar interaction being independent of the many-hole effects. On the other hand, ordering of macroscopically hole-rich regions is in agreement with the conjecture that all ground states are geometrically ordered.[46]

On increasing $B>0$, at fixed density, the Wigner crystal becomes unstable and a new phase with diagonal stripes is formed, as shown in Fig. 2a of Ref. 47. The main characteristic of this phase is a ferromagnetic ordering of the AF dipoles. The situation here is very similar to that observed in $La_{2-x}Sr_xNiO_{4+y}$ (see Ref. 7). Note that such a state with a dipole ordering appears to violate time-reversal symmetry. On the other hand, the true ground state in this case also involves hole ordering, with holes aligned in stripes either perpendicular or parallel to the dipole orientation. However, the interstripe distance, in this case, is close to that between holes within a stripe and hence a simulation inevitably yields a ''glassy'' state, with many defects. This is reflected in the shape of ρ_k, which shows broad peaks (see Fig. 2(b) in Ref. 47), indicating an average interstripe distance.

As shown in Fig. 3(a), at larger values of B a linear stripe is formed, which, with increasing density tends to close into a loop. More importantly, the loop formation is accompanied by magnetic dipole orientation along the straight portion of a loop with gradual rotation by $\pi/2$ at each corner.[48] Due to the rotation of dipoles at corners, the loops interact and eventually form the checkerboard (grid) pattern.[49] The size of the distance between holes within a line is determined by the ratio of B (or the sum of A and B, for $A\neq B$) and the Coulomb energy; the grid sizes are determined by the hole density alone. These results appear to be consistent with the DMRG numerical solution of the t-J model[25] which also finds loops of holes, except that in our case the periodic boundary conditions and the Coulomb interaction yield a ''tile grid'' as opposed to ''droplets.'' Note the almost perfect (infinite charge correlation length, ξ_c) crystal structure obtained [Fig. 3(c)]. It is noteworthy that a typical solution yields a finite dipole moment at each grid intersection, which, in turn, can take one of the two orientations (along two diagonals of the computational box), thus creating a highly degenerate system of moments (see Fig. 6 below).

We recall that the presented solution is obtained assuming an arbitrary dipole orientation with a constant hole dipole magnitude, i.e., a continuum of angles between the dipoles and a fixed axis. As explained in the previous section, at very low doping the dipoles would reside near the Brillouin zone (BZ) diagonals, i.e., they would assume almost ''discrete'' orientations. In order to study the effect of this ''discreteness'' we have performed the same simulation this time, assuming that hole dipoles can take only one of four directions (determined by the momenta of the maxima of the lower Hubbard band). We find that the physics of the pattern formation is qualitatively unaltered (hence we do not present them here), except for one important difference: the ''bending'' of stripes at the grid intersections disappears, i.e., one no longer has a finite dipole moment at these intersections.

Another way of quantifying this ordered phase is by straightforwardly calculating the ''string tension,'' which at $T\rightarrow 0$ is equal to $\partial^2 U/\partial x^2$, where U is the total potential energy and x is a small hole (or stripe) displacement; a large string tension indicates a high stability of the obtained phase, and vice versa. In Fig. 4(a) we show the string tension for

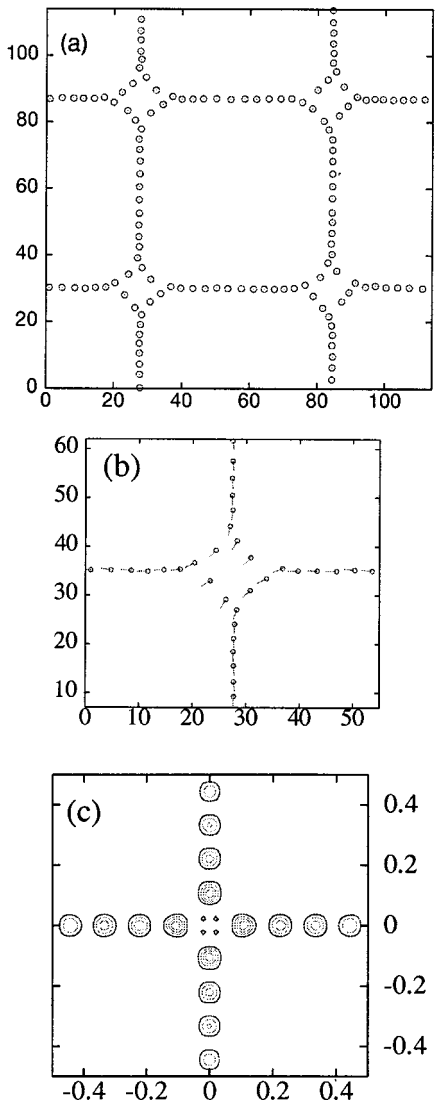

FIG. 3. Low-T state for larger finite values of $B, B=4$ eV, at $n=15\%$ doping level. The holes (circles) form a grid [Ref. 47 (panel (a)] with dipoles orientated along line segments and a dipole rotation at grid intersections [panel (b)]. Panel (c) shows a contour plot of the average charge density ρ_k in arbitrary units, indicating ''perfect'' geometric order. (Ref. 47) Even after averaging over many solutions in this case the charge peaks are much sharper than those found in the ferrodipolar phase (see Fig. 2(b) in Ref. 47).

motion perpendicular to a grid side compared with the motion along a side. As seen in the figure, the grid phase (and, as discussed below, the stripe phase) is extremely stable with respect to the hole motion perpendicular to the holes line segments, due to the Coulomb interacton. On the other hand, at larger doping values and fixed hole density the stripes are almost compressible, i.e., the motion of holes along a stripe is rather soft. The anisotropy of the perpendicular and longitudinal string tension decreases with decreasing B.

At fixed AF correlation length the four observed phases yield a diagram that we show in Fig. 5(a). We remark that in all phases a nonvanishing value of A leads to a decrease in the effective value of B at which the transitions occur, as shown in Fig. 5(b). The isotropic term A alone *never* produces any nontrivial geometric phase (e.g., stripes), even with inclusion of lattice effects. We find that the transition

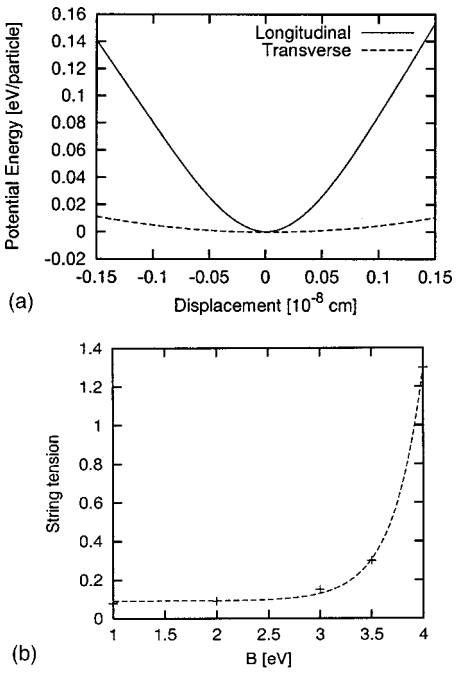

FIG. 4. (a) Energy as a function of a hole position, reflecting the string tension in the stripe, for $B=4$ eV and $n=15\%$. Clearly, the motion of holes perpendicular to the the grid directions is quite hard and while the motion along a line stripe is much softer (see also text). (b) average string tension as a function of B, at $n=15\%$. Note the almost exponential dependence (solid line) up to the critical value of $B\sim 4$ eV where the system undergoes the first-order transition between the ferrodipolar and grid phases.

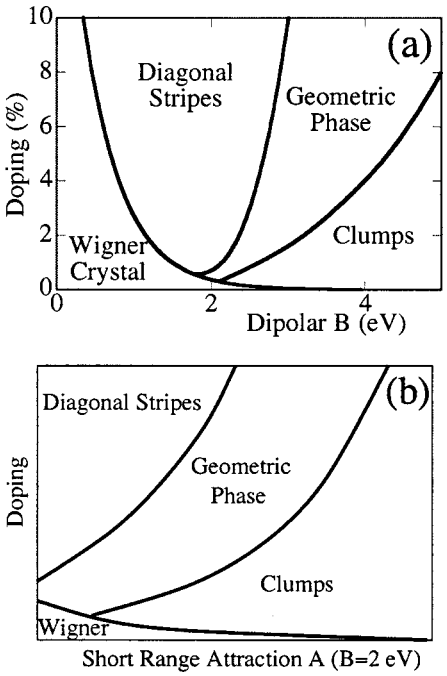

FIG. 5. (a) $A=0$, n-B phase diagram (from Ref. 47). (b) Fixed B,n-A phase diagram. It is noteworthy that the experimentally relevant values of A and B are of order ~ 1 eV. The slightly higher values of B, at which we find geometric (grid and stripe) phases, are due to the fact that we consider unscreened Coulomb interaction and in reality they would be considerably smaller (see also Fig. 9).

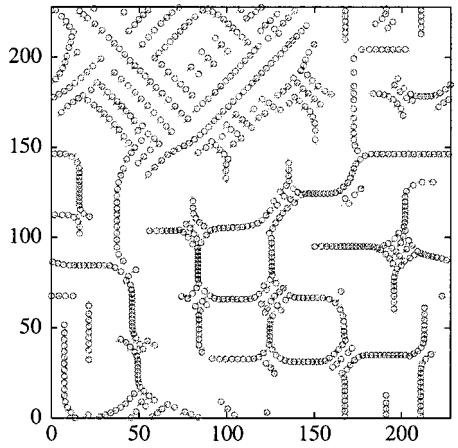

FIG. 6. Coexistence of dipolar and grid phases, indicating the first-order nature of the transition between them.

between the ferrodipolar and the grid phases is first order, as indicated by the coexistence of phases in Fig. 6. Note that this transition always occurs on increasing the doping level to sufficiently (and artificially) high values, where our theory need not apply. No coexistence of phases has been observed at other transitions, suggesting that they are second order. We also recall that our calculations are *quasiclassical* and thus the obtained geometric (stripe) phases are insulating. Moreover, in our formalism the hole density within a stripe can assume an arbitrary value, depending on the dipolar interaction strength.

In the cases presented above we have assumed a uniform magnetic dipolar interaction. It is well known that there are orthorhombic and tetragonal distortions in practically all transition metal oxides. In particular static stripe formation has only been observed in the low-temperature tetragonal phase of $La_{1.6-x}Nd_{0.4}Sr_xCuO_4$.[9] In order to study the influence of the anisotropy we assume that the magnetic dipole sizes along the x and y directions have anisotropy α ($\alpha=1$ corresponds to the isotropic case). Figure 7 shows the pattern we obtain for $\alpha=0.8$

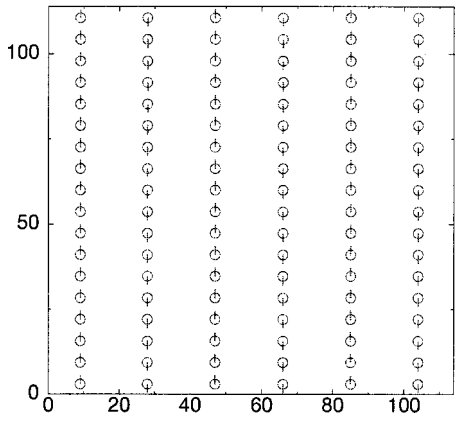

FIG. 7. With a small x-y directional anisotropy in the dipolar interaction, Eq. (6), with the anisotropy parameter $\alpha=0.8$ (in the uniform case $\alpha=1$), the holes (shown by circles) form a stripe rather than a grid pattern. Note the hole dipole orientations (shown by the line segments), altering direction in neighboring stripes, corresponding to the π phase shift of the local magnetization between magnetic domains separated by stripes. (Ref. 22).

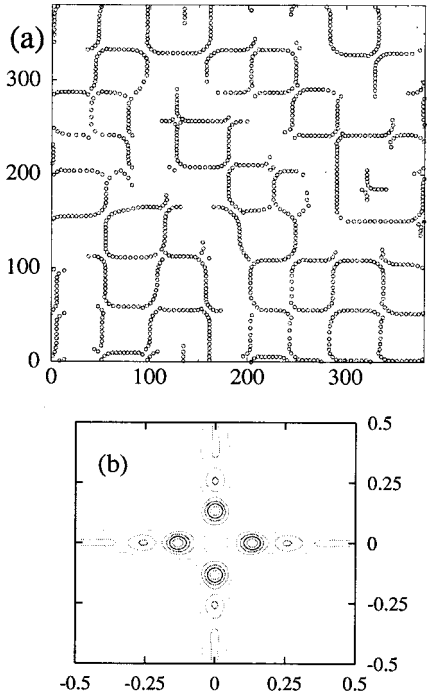

FIG. 8. (a) A typical low-energy state in a larger computational box, obtained for the same value of B and n as in Fig. 3. Note the presence of point and line defects. It is important to realize that the average size of the grid units depends only on the physical parameters and very weakly on the size of the computational box. (b) The charge density ρ_k averaged over a number (of order 10) of hole configurations. Note that the peak positions are the same as those shown in Fig. 3, but due to the presence of defects the intensity of the higher Bragg peaks vanishes.

The rotational symmetry is broken and a stripe superlattice is formed, with a charge ordering vector $\mathbf{K}=(2\pi/l)\mathbf{x}$, where l is the interstripe distance. More importantly, the total dipole moment in this state vanishes. As explained in Sec. II, this yields a Fourier transform of the magnetization $S(\mathbf{q})=\langle S_z(\mathbf{q})\rangle$ peaked at $\mathbf{Q}\pm\mathbf{K}$ in momentum space. Of course, it is reasonable to assume that in twinned single crystals, used in inelastic neutron scattering experiments, one has domains that average out this anisotropy. Note that in both calculated geometric phases (see Figs. 3 and 7), the interstripe distance is much larger than the intrastripe distance, in agreement with experimental findings in underdoped cuprates.

Our results are somewhat sensitive to the applied boundary conditions. First, for a small computational box the exact size of the grid depends on its commensuration with the box length, which, in turn depends on the density. On increasing of the size of the computational box, the grid size depends only on the physical parameters, as explained below Fig. 3. In addition, for a large computaitonal box the grid pattern, shown in Fig. 3(a), acquires point or line defects, shown in Fig. 8(a).

This leads to the reduction in the higher order peaks observed in Fig. 3(b) with no change in their wave numbers, indicating the finite value of ξ_c, as seen in Fig. 8(b). The sensitivity to boundary conditions is further seen in finite size calculations, i.e, not assuming periodic boundary conditions, but with an appropriate neutralizing charge background. In this case the holes do not form geometric phases,

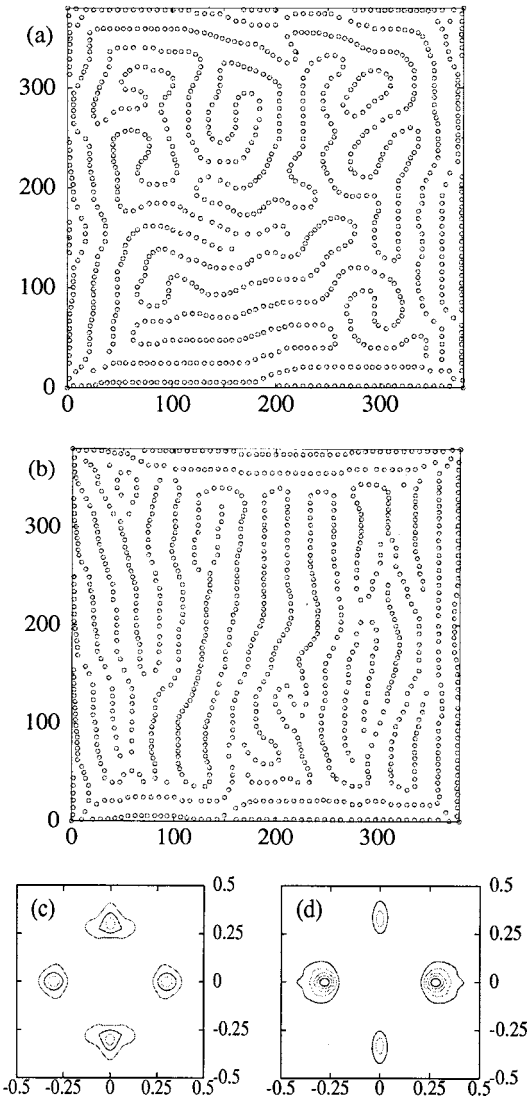

FIG. 9. (a) A typical low-T metastable state of the hole system, obtained *without* periodic boundary conditions and with an appropriate positive background included. While the ground state is still a geometrically ordered state, it is practically unreachable due to the presence of many metastable states. (b) Adding very small directional anisotropy [$\alpha=0.9$, with $\alpha=1$ corresponding to the uniform case shown in panel (a); see also Fig. 7] yields stripes with some defects. Panels (c) and (d) show ρ_k as a function of momentum corresponding to the results shown in panels (a) and (b), respectively.

although they still form stripes, as seen in Fig. 9(a). However, in a finite system even very small anisotropy ($\alpha\sim0.95$) again leads to stripe formation, as seen in Fig. 9(b). It is worth mentioning that the stripe formation occurs for much smaller values of B and the same density and AF correlation length in a finite system.

We have also performed simulations in the presence of a realistic underlying periodic lattice and have found that this creates slight distortions in the phases, pinning loops more strongly. In particular, the peaks in $\rho(\mathbf{q})$ sharpen in some of these phases.

A. Role of disorder

We now turn to the effects of point disorder. There are several kinds of impurities that are of experimental interest

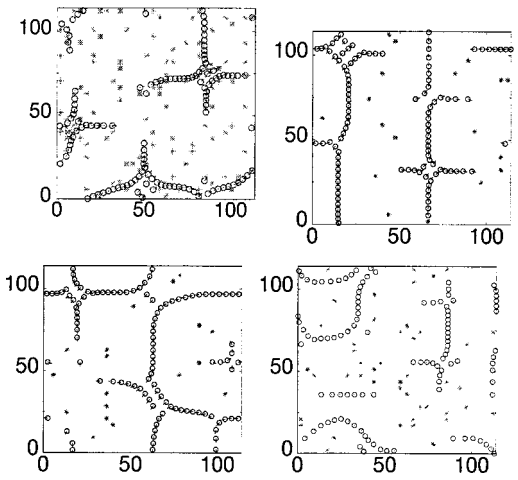

FIG. 10. The effects of impurities of different types. The four panels show hole (circles) and impurity (stars) positions, for the case of charged impurities, placed $d=6$ Å out-of-plane (top left), in-plane repulsive uncharged impurities (top right), in-plane repulsive charged impurities (bottom left), and in-plane impurities with a local magnetic moment that destroys local AF ordering (bottom right). Clearly, all impurities destroy the stripe order, although the out-of-plane impurities and the uncharged in-plane impurities are nearly as effective as the in-plane charged impurities. The latter lead to the a glassy phase of stripe segments at relatively low concentrations, of order a few percent.

in transition metal oxides. We divide them into four distinct groups: (I) out-of-plane impurities, such as Sr in $La_{2-x}Sr_xCuO_4$ compounds, (II) in-plane charged impurities, such as (presumably) Li,[50] (III) in-plane uncharged impurities, such as Ni, and (IV) in-plane uncharged impurities that induce a magnetic moment, such as Zn. Hence, we model the impurity effects by adding a random (in position) potential to the Hamiltonian (7), which is either short-ranged and located in-plane or, as in the case of charged impurities, long-ranged (Coulomb) and either in-plane or out-of-plane (a distance d from the plane where the holes are located). In the case of type IV we have also altered the dipolar interaction in the vicinity of an impurity, i.e., the magnetic interaction is multiplied by a factor $\tanh(r/R_i)$, where r is the distance of a hole to a nearby impurity and R_i is the effective radius of the impurity, which, for the case of Zn, has been estimated to be of order 2 lattice sites around each impurity atom.[51] Examples of the effects of the four types of impurities are presented in Fig. 10.

Clearly, all four types of impurities lead to the destruction of the geometric (stripe or grid) hole order at sufficiently large impurity concentration, c_i. On the other hand, in all four cases stripe ordering persists through the formation of line segments of holes, resulting in a new, *glassy* phase.[52] Moreover, the four impurity types exhibit different mechanisms for destroying the stripe order. The charge ordered phases are practically unaffected by a small concentration of uncharged impurities [see Fig. 10(b)], i.e., the stripes simply avoid impurity sites. Consequently, the stripes persist to relatively high concentrations of this type of disorder.

The charged impurities first lead to stripe deformation, i.e., the stripes pass either very close to the impurities (for attractive, pinning impurities) or very far from the impurities (for repulsive impurities), in order to maximize the potential

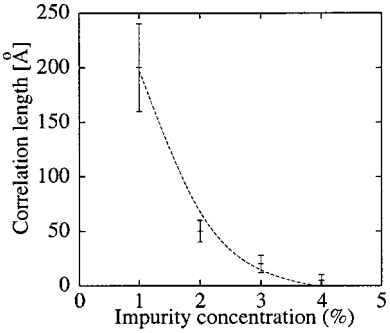

FIG. 11. Zero temperature *charge* correlation length as a function of impurity concentration for the in-plane charged impurity case: the result is obtained by measuring the static correlation length, and then averaging over many (of order 20) different impurity configurations.

energy [see Figs. 10(a) and 10(c)]. With increasing c_i the stripes rupture and only stripe segments persist. Finally, the impurities with a local magnetic moment affect the formation of the spiral spin phase, responsible for the (attractive) dipolar interaction. Since the magnetic interaction is strongly suppressed in the vicinity of such an impurity site, even the stripe segments cannot exist there, as shown in Fig. 10(d).

Impurities are especially effective in destroying the ordered phases found at small B. For example, the Wigner crystal state becomes glassy at relatively low impurity concentrations. This happens because, e.g., in the case of impurity type I, the attractive Coulomb energy between impurities and holes scales like e^2/d, where d is the distance between the planes in which the impurities and holes reside, while the average interhole Coulomb energy behaves a $e^2\sqrt{\sigma_s}$. Thus when $\sigma_s < 1/d^2$ the holes are pinned by impurities.

In general the role of impurities depends strongly on the impurity concentration, c_i. However, the magnetic dipole interaction is sufficient to retain the main orientation, as seen in Fig. 11, where we have plotted the correlation length as a function of c_i. This leads us to conjecture that with the addition of the kinetic energy the holes can move in string segments in an orientation given basically by the phase diagram of the clean system. The stripe motion would then be caused by mesoscopic thermal or quantum tunneling of the finite strings between the minima of the overall potential. This would lead to nonlinear field dependence in the low-temperature conductivity.[53]

B. Finite-temerature results

We now proceed to the finite-T results. The numerical procedure is identical, except that the temperature is lowered adiabatically to a finite value (i.e., a numerical annealing). In a classical simulation this is equivalent to introducing kinetic energy into the system.

In the case of a Wigner crystal, $B=0$, we find that the introduction of finite T melts the crystalline structure and the resulting phase is the 2D Coulomb gas. The diagonal (glassy) phase is also unstable at relatively low temperatures. On the other hand, the geometrically ordered states, for $a_s \ll \xi$, where a_s is the distance between holes within a stripe segment, are all stable up to T of order $\sim B/\sigma_s a_s^2$. At even higher temperatures, the stripe array melts with a temporal

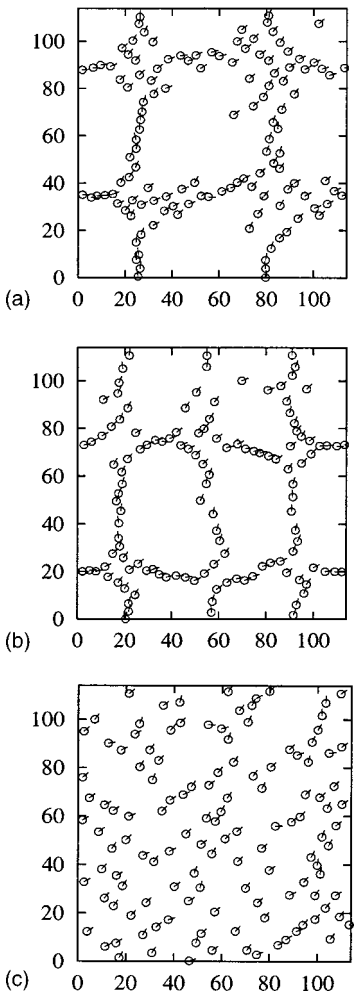

FIG. 12. Spatiotemporal intermittent behavior of hole ordering *near the melting transition*: three snapshots are shown. (a) corresponds to a state that is clearly withing the basin of attraction of the ground state (the same pattern, albeit deformed), while panel (b) shows a state that is within the basin of attraction of another low-lying geometric state with more dense stripes along one of the axis. Panel (c) shows the melted *nematic crystal*–like phase with the hole dipole moments aligned.

intermittency of the observed pattern: i.e., spatiotemporal intermittency. Figure 12 shows three stages of this melting process. We observed that the stripe melts through a rupture, which results in the creation of finite stripe segments that eventually (at constant and high T) disperse into individual holes.

Note that the temporal geometric pattern [panel (b)] is not the same as that in the ground state. As mentioned before, there are many low-lying geometric states, close in energy to the ground state, which can temporarily occur at finite T. Hence the dynamics of the stripe ordering is similar to that observed in glasses, characterized by non-Gaussian fluctuations. To show this we follow the dynamics of the hole system at temperatures slightly *below* the melting temperature: we start from a low-lying metastable state, such as that depicted in Fig. 12(b), increase the temperature adiabatically to the point at which the structure begins to melt (which is a measure of the activation energy) and let the system equilibrate.

In Fig. 13(a) we plot an energy histogram at this temperature (with the energy shifted by an arbitrary additive constant), thus indicating an intensity of the energy states (bands). Obviously, there is a band of energy states, not far (fraction of an eV per particle) from the ground state, which are close in energy and metastable. These states are separated by a high barrier (the maximum of which would fall beyond the right edge on the plot), yet are close in energy, suggesting a *rugged* energy landscape.[55] Indeed, as shown earlier, formation of a string of holes creates a barrier for adding more holes to the string (they can be only added to the string ends). Thus, any geometrically ordered state (say, those with denser intrastripe hole concentration and larger interstripe distances) must be separated by an energy barrier from other geometrically ordered states and in particular from the ground state.

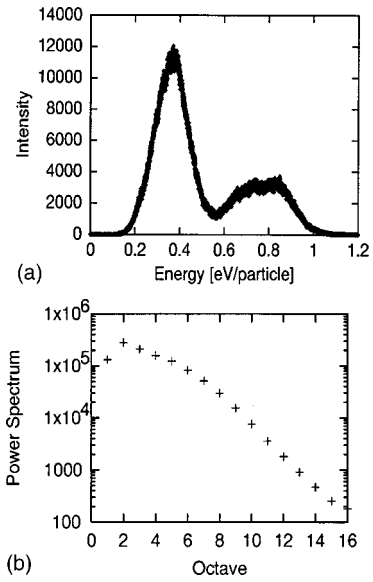

FIG. 13. (a) a histogram of the energies at constant (high) temperature of order of the activation energy for a transition between the two energy basins, depicted by the states shown in Fig. 12. The left maximum corresponds to the ground state, Fig. 12(a), and the right to a family of low-lying excited states, Fig. 12(b). Neither peak can be fitted by a simple Gaussian, indicating a glassy nature of the ordered states. (b) The average ''power spectrum'' corresponding to the result shown in (a): the vertical axis shows the sum of the squares of the Fourier components of the potential energy, within the nth octave (components 2^{n-1} through 2^n-1, for $n>0$), averaged over many (of order 300) spectra. The flat low-frequency behavior (up to about the 9th component) is very close to a generic (Ref. 54) $1/f$ noise and corresponds to slow fluctuations involving many particles, such as those yielding the transitions between the states depicted in Figs. 12(a) and 12(b).

The potential energy states obtained suggest that the dynamics of stripe motion should be strongly governed by these low-lying states and thus show a nontrivial fluctuation spectrum. Indeed, in Fig. 13(b) we show the power spectrum of the energy fluctuations for the solution described by the histogram in Fig. 13(a), and see that the noise spectrum contains a strong $1/f$ component for approximately two and half decades of frequencies. This indicates slow fluctuations, which we ascribe to collective motions of melted hole string segments.

Another way of characterizing the melting of stripes is by counting ''free holes.'' In Fig. 14 we show the percentage of

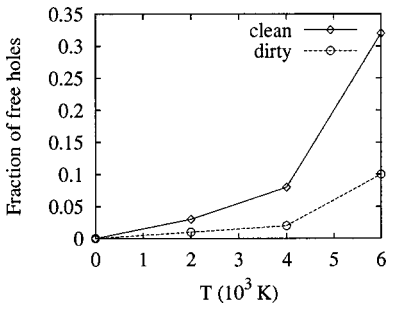

FIG. 14. Percentage of holes that are *not* a part of a stripe segment, as a function of temperature, for $B=4$ eV.

holes that are *not* in a part of an ordered pattern, as a function of T. As one can see, at the transition point only a small fraction of holes does not belong to a string segment, in agreement with our observation that the stripes melt by rupturing into smaller segments. Further study of the glassy dynamics of charge ordered phases in terms of the (free) energy landscape will be presented elsewhere.

IV. CONCLUSIONS

In summary, on employing the SDW picture of transition metal oxides, we have studied the short-range and dipolar attractive forces generated by the AF fluctuations, together with long-range Coulomb forces. We have developed a numerical technique, that enables us to treat doped hole vacancies at finite concentration. We have studied the competition between long-range and short-range interactions and its influence on hole ordering in layered transition metal oxides. We have found a rich phase diagram for the clean system, which includes a Wigner solid, diagonal stripes, a grid (loops), and a macroscopic phase separation. For intermediate values of magnetic interaction this phase diagram is consistent with several different experimental measurements, such as inelastic neutron scattering. In addition, on adding a small, but finite amount of anisotropy to the dipolar interaction we find that the ground state of the system of holes is the striped phase, found in $La_{2-y-x}Nd_ySr_xCuO_4$. In the geometric phases with strong magnetic interaction strength we have found a large string tension for the motion of holes perpendicular to the stripe direction. This is due to the Coulomb interaction and indicates strong stability of the obtained phases.

We have also found the system of holes to be quite sensitive to the presence of charged impurities. In particular, adding out-of-plane attractive impurities pins the holes and, for small pinning energies, increases the melting temperature of the stripe phase, although it does yield a finite charge correlation length. In general, charged impurities are very effective in destroying the stripe order, especially those residing in the same plane as the holes, regardless of whether they are attractive or repulsive, although the stripe phases survive as finite *stripe segments* up to relatively high impurity concentrations. This suggests that nonlinear conductivity should be prevalent.

The resulting hole patterns are the result of frustration (competition between short-range and long-range forces): this frustration leads to collective motions, involving large number of particles that ultimately lead to geometrically ordered ground states. We have also studied the dynamics of the geometric phase formation and its melting. We find that the dynamics is characterized by a ''glassy'' behavior in that the energy landscape is rugged, as characterized by the spatiotemporal intermittency of the observed behavior. More importantly, we find that, for a fixed (large) size of the magnetic (dipolar) interaction, there are fewer number of sharper minima, while the string tension of the stripes is larger. As a consequence, in this case the melting of the stripe phase occurs at higher temperature with increased doping concentration.

The energy landscape is also characterized by formation of domains, separated by defects. This picture is in agreement with recent NMR experiments[11] in which small activation energies are easily attributed to domain growth and/or motion. Thus, further study of our model will include the dynamics of the domain growth and their melting.

ACKNOWLEDGMENTS

We gratefully acknowledge valuable discussions with A. Balatsky, A. Chubukov, N. Curro, J. Gubernatis, C. Hammel, G. Ortiz, D. Pines, D. Scalapino, J. Schmalian, S. White, and J. Zaanen. A. H. C. N. acknowledges support from the Alfred P. Sloan Foundation. Work at Los Alamos was supported by the U. S. Department of Energy. Work at the University of California, Riverside, was partially supported by a Los Alamos CULAR project. Work at Lawrence Berkeley Laboratory was partly supported by the Director, Office of Advanced Scientific Computing Research Division of Mathematical, Information, and Computational Sciences of the U.S. Department of Energy under Contract No. DE-AC03-76SF00098.

APPENDIX A: MAGNETIC DIPOLES OF THE HUBBARD MODEL

In this appendix we study the Hubbard model, Eq. (1), in the SDW state. Our approach is similar to that presented in Refs. 28 and 35. Hence we only briefly review the calculation leading to Eq. (5), the central equation of the paper.

The relevant order parameter in our case is the spin density in the z direction:

$$S^z(\mathbf{q})=\sum_{\mathbf{k},\alpha}\ \alpha c^{\dagger}_{\mathbf{k}+\mathbf{q},\alpha}c_{\mathbf{k},\alpha}, \tag{A1}$$

which in the SDW state has a finite expectation value at $\mathbf{q}=\mathbf{Q}=(\pi/a,\pi/a)$ because of the nesting of the half-filled Fermi surface. In this case the mean-field Hamiltonian reads

$$H_{MF}=\sum_{\mathbf{k},\alpha}\ \epsilon_k c^{\dagger}_{\mathbf{k},\alpha}c_{\mathbf{k},\alpha}-\frac{USN}{2}\sum_{\mathbf{k},\alpha}\ \alpha c^{\dagger}_{\mathbf{k}+\mathbf{Q},\alpha}c_{\mathbf{k},\alpha}, \tag{A2}$$

where

$$S=\frac{1}{N}\langle S^z(\mathbf{Q})\rangle,$$

$$\epsilon_k=-2t[\cos(k_xa)+\cos(k_ya)]. \tag{A3}$$

The Hamiltonian (A2) can be diagonalized immediately using the Bogoliubov transformation:

$$\gamma^c_{\mathbf{k},\alpha} = u_{\mathbf{k}} c_{\mathbf{k},\alpha} + \alpha v_{\mathbf{k}} c_{\mathbf{k}+\mathbf{Q},\alpha},$$

$$\gamma^v_{\mathbf{k},\alpha} = v_{\mathbf{k}} c_{\mathbf{k},\alpha} - \alpha u_{\mathbf{k}} c_{\mathbf{k}+\mathbf{Q},\alpha}, \tag{A4}$$

where

$$u_{\mathbf{k}} = \sqrt{\frac{1}{2}\left(1+\frac{\epsilon_k}{E_k}\right)},$$

$$v_{\mathbf{k}} = \sqrt{\frac{1}{2}\left(1-\frac{\epsilon_k}{E_k}\right)},$$

$$E_k = \sqrt{\epsilon_k^2+\Delta^2},$$

$$\Delta = -\frac{US}{2}. \tag{A5}$$

In this case the mean-field Hamiltonian reads

$$H_{MF} = \sum_{\mathbf{k},\alpha} E_k (\gamma^{c\dagger}_{\mathbf{k},\alpha}\gamma^c_{\mathbf{k},\alpha} - \gamma^{v\dagger}_{\mathbf{k},\alpha}\gamma^v_{\mathbf{k},\alpha}), \tag{A6}$$

where the sum over $\mathbf{k}$ is restricted to the magnetic Brillouin zone and, at half filling, the ground state $|0\rangle$ is defined such that

$$\gamma^c_{\mathbf{k},\alpha}|0\rangle = 0,$$

$$\gamma^{v\dagger}_{\mathbf{k},\alpha}|0\rangle = 0. \tag{A7}$$

Thus, at half filling the conduction band is empty and the valence band is separated from it by energy Δ, which is the Mott-Hubbard gap. It is known that this theory recovers the results of the Heisenberg model very well. Consider, for instance, the average spin density in Eq. (A1) in terms of the new operators (recall that the conduction band is empty and therefore does not contribute)

$$\langle S^z(\mathbf{q})\rangle = -2\sum_{\mathbf{k},\alpha} u_{\mathbf{k}+\mathbf{q}-\mathbf{Q}} v_{\mathbf{k}} \langle \gamma^{v\dagger}_{\mathbf{k}+\mathbf{q}-\mathbf{Q},\alpha}\gamma^v_{\mathbf{k},\alpha}\rangle$$

$$= -4\delta_{\mathbf{q},\mathbf{Q}}\sum_{\mathbf{k}} u_{\mathbf{k}} v_{\mathbf{k}}$$

$$= -4\delta_{\mathbf{q},\mathbf{Q}}\sum_{\mathbf{k}} \frac{\Delta}{2E_k}, \tag{A8}$$

which, together with Eq. (A5), yields the gap equation:

$$\frac{1}{N}\sum_{\mathbf{k}} \frac{1}{\sqrt{\epsilon_k^2+\Delta^2}} = \frac{1}{U}. \tag{A9}$$

Since we are going to consider hole doping we can neglect the terms involving the conduction band operators for temperatures $T \ll \Delta$. As shown in Ref. 28 new interactions are generated by the antiferromagnet in the presence of the holes, given by H_z and H_{xy}. The noninteraction hole Hamiltonian is, from Eq. (A6),

$$H_0 = -\sum_{\mathbf{k},\alpha} E_k \gamma^{v\dagger}_{\mathbf{k},\alpha}\gamma^v_{\mathbf{k},\alpha}. \tag{A10}$$

Close to the half-filled Fermi surface one sees that the hole mass is

$$m_h \approx \frac{\Delta}{8t^2 a}. \tag{A11}$$

For any state $|\Psi\rangle$ of the system we can define the hole operators as

$$\gamma^v_{\mathbf{k},\alpha}|\Psi\rangle = h^\dagger_{-\mathbf{k},-\alpha}|\Psi\rangle \tag{A12}$$

in which case the Hamiltonian reads

$$H_0 = \sum_{\mathbf{k},\alpha} E_k h^\dagger_{\mathbf{k},\alpha} h_{\mathbf{k},\alpha} \tag{A13}$$

plus unimportant constants.

The interacting parts of the Hamiltonian can also be written in terms of this new operators. For instance,

$$H_z = \frac{1}{N}\sum_{\mathbf{k},\alpha} \{[[V_z(\mathbf{Q}) - V_z(2\mathbf{k}-\mathbf{Q})/4]m^2_{k,k} - V_z(2\mathbf{k})l^2_{k,k}/4]\}$$

$$\times h^\dagger_{\mathbf{k},\alpha}h_{\mathbf{k},\alpha} - \frac{1}{4N}\sum_{\mathbf{k},\mathbf{k}'} [V_z(\mathbf{k}-\mathbf{k}')l^2_{k,k'}h^\dagger_{\mathbf{k},\alpha}\sigma^z_{\alpha,\alpha'}h_{\mathbf{k}',\alpha'}$$

$$\times h^\dagger_{-\mathbf{k},\beta}\sigma^z_{\beta,\beta'}h_{-\mathbf{k}',\beta'} + V_z(\mathbf{k}-\mathbf{k}'+\mathbf{Q})$$

$$\times m^2_{k,k'}h^\dagger_{\mathbf{k},\alpha}h_{\mathbf{k}',\alpha}h^\dagger_{-\mathbf{k},\beta}h_{-\mathbf{k}',\beta}], \tag{A14}$$

where the sum over spin indices is implicit and

$$V_z(q) = \frac{U^2\chi^z_0(q)}{1-U\chi^z_0(q)}, \tag{A15}$$

with

$$\chi^z_0(q,\omega) = -\frac{1}{2N}\sum_{\mathbf{k}}\left(1-\frac{\epsilon_k\epsilon_{k+q}+\Delta^2}{E_kE_{k+q}}\right)$$

$$\times\left(\frac{1}{\omega-E_{k+q}-E_k} - \frac{1}{\omega+E_{k+q}+E_k}\right). \tag{A16}$$

A similar expression is valid for the transverse components of the interaction

$$H_{xy} = -\frac{4}{N}\sum_{\mathbf{k},\alpha}(1-\alpha)[V_{+-}(2\mathbf{k})n^2_{k,k} - V_{+-}(\mathbf{Q}+2\mathbf{k})p^2_{k,k}]$$

$$\times h^\dagger_{\mathbf{k},\alpha}h_{\mathbf{k},\alpha} - \frac{1}{4N}\sum_{\mathbf{k},\mathbf{k}'}[V_{+-}(\mathbf{k}-\mathbf{k}')n^2_{k,k'}$$

$$- V_{+-}(\mathbf{k}-\mathbf{k}'+\mathbf{Q})p^2_{k,k'}]h^\dagger_{\mathbf{k},\alpha}\sigma^+_{\alpha,\alpha'}h_{\mathbf{k}',\alpha'}$$

$$\times h^\dagger_{-\mathbf{k},\beta}\sigma^-_{\beta,\beta'}h_{-\mathbf{k}',\beta'}, \tag{A17}$$

where V_{+-} is given by an expression similar to Eq. (A15) with χ^z_0 replaced by

$$\chi_0^{+-}(q,\omega)=-\frac{1}{2N}\sum_{\mathbf{k}}\left(1-\frac{\epsilon_k\epsilon_{k+q}-\Delta^2}{E_kE_{k+q}}\right)\left(\frac{1}{\omega-E_{k+q}-E_k}-\frac{1}{\omega+E_{k+q}+E_k}\right). \tag{A18}$$

Moreover, the coefficients that appear in these expressions are defined by

$$m_{k,k'}=u_kv_{k'}+v_ku_{k'},$$
$$l_{k,k'}=u_ku_{k'}+v_kv_{k'},$$
$$p_{k,k'}=u_kv_{k'}-v_ku_{k'},$$
$$n_{k,k'}=u_ku_{k'}-v_kv_{k'}. \tag{A19}$$

Observe that the interactions renormalize the dispersion of the holes as well, that is, $E_k\rightarrow E_k^R$. While H_z is essentially a short-range attractive interaction in the spin-symmetric channel, H_{xy} has two components: one of them is also an attractive interaction in the spin-symmetric channel but the other is a long-range dipolar interaction, which depends on the momentum of the hole.

The Hamiltonian, which consists of terms given by Eqs. (A14) and (A17), is very difficult to deal with. One notices, however, that the mean-field energy E_k is degenerate along the magnetic Brillouin zone. This is an artifact of the theory and the degeneracy is broken by any small perturbation such as the corrections discussed before or a next nearest hopping, t', for instance. In this case, the dispersion has a minimum at $(\pm\pi/2,\pm\pi/2)$. Thus, in order to study the long-wavelength limit of the theory it is sufficient to focus on these points of the Brillouin zone. In the paper by Schrieffer, Wen, and Zhang[28] the authors focused entirely on the H_z part of the Hamiltonian since the form factors $n_{k,k'}$ and $p_{k,k'}$ vanish at the Brillouin zone. As shown by Frenkel and Hanke,[29] if one keeps the leading order in momentum we can write

$$p_{k,k'}\approx\frac{t}{\Delta}|(k_x-k_x')+(k_y-k_y')|,$$
$$V_{+-}(\mathbf{q}+\mathbf{Q})\approx\frac{1}{t^2}\frac{1}{q^2}, \tag{A20}$$

and therefore the interaction term becomes

$$V_{+-}(\mathbf{q}+\mathbf{Q})p_{k,k+q}^2\approx 2U\frac{(q_x+q_y)^2}{q^2}=2U\left(1+2\frac{q_xq_y}{q^2}\right), \tag{A21}$$

which has dipolar form.

Thus, in the first quantized language the interactions have the form

$$H_I\approx\{A\sigma^z(\mathbf{r}_1)\sigma^z(\mathbf{r}_2)-B[\sigma^+(\mathbf{r}_1)\sigma^-(\mathbf{r}_2)+\sigma^-(\mathbf{r}_1)\sigma^+(\mathbf{r}_2)]\}\times\delta(\mathbf{r}_1-\mathbf{r}_2)-C\frac{xy}{r^4}[\sigma^+(\mathbf{r}_1)\sigma^-(\mathbf{r}_2)+\sigma^-(\mathbf{r}_1)\sigma^+(\mathbf{r}_2)], \tag{A22}$$

where σ are spin operators. Notice that the singlet state $|\uparrow,\downarrow\rangle-|\downarrow,\uparrow\rangle$, clearly minimizes the energy of interaction between the two holes. In this case we end up with the charge interactions only.

From our simulations we see that the charge orders with some characteristic vector $\mathbf{K}$ such that

$$\rho(\mathbf{q})=\sum_{\mathbf{k},\alpha}h^\dagger_{\mathbf{k}+\mathbf{q},\alpha}h_{\mathbf{k},\alpha} \tag{A23}$$

acquires a finite expectation value at $\mathbf{q}=\mathbf{K}$. Thus, we can always write down a mean-field version of Eq. (A22) plus the long-range Coulomb interaction as

$$H_I=-\frac{\rho N}{2}\sum_{\mathbf{k},\alpha}V_kh^\dagger_{\mathbf{k}+\mathbf{K},\alpha}h_{\mathbf{k},\alpha}, \tag{A24}$$

where V_k has to be calculated from Eqs. (A14) and (A17) and

$$\rho=\frac{1}{N}\langle\rho(\mathbf{K})\rangle. \tag{A25}$$

Observe that in this case the Brillouin zone is further reduced and we can define new operators

$$d^+_{\mathbf{k},\alpha}=w_kh_{\mathbf{k},\alpha}+t_kh^\dagger_{\mathbf{k}+\mathbf{K},\alpha},$$
$$d^-_{\mathbf{k},\alpha}=t_kh_{\mathbf{k},\alpha}-w_kh^\dagger_{\mathbf{k}+\mathbf{K},\alpha}, \tag{A26}$$

with

$$w_k=\sqrt{\frac{1}{2}\left(1+\frac{E_k^R}{E_k^T}\right)},$$
$$t_k=\sqrt{\frac{1}{2}\left(1-\frac{E_k^R}{E_k^T}\right)}, \tag{A27}$$
$$E_k^T=\sqrt{(E_k^R)^2+\frac{(\rho V_k)^2}{4}},$$

and the Hamiltonian is diagonal,

$$H=\sum_{\mathbf{k},\alpha}E_k^T(d^{+\dagger}_{\mathbf{k},\alpha}d^+_{\mathbf{k},\alpha}-d^{-\dagger}_{\mathbf{k},\alpha}d^-_{\mathbf{k},\alpha}), \tag{A28}$$

where the sum is done in the new Brillouin zone. Self-consistency requires that

$$\rho=\frac{1}{N}\sum_{\mathbf{k},\alpha}w_kt_k(\langle d^{+\dagger}_{\mathbf{k},\alpha}d^+_{\mathbf{k},\alpha}\rangle-\langle d^{-\dagger}_{\mathbf{k},\alpha}d^-_{\mathbf{k},\alpha}\rangle), \tag{A29}$$

which can be evaluated for any hole-filling.

Now let us go back to the issue of magnetization which is important for neutron scattering. From Eq. (A8) one has

$$\langle S^z(\mathbf{q})\rangle = -2\sum_{\mathbf{k},\alpha} u_{\mathbf{k}+\mathbf{q}-\mathbf{Q}} v_{\mathbf{k}} \langle \gamma^{v\dagger}_{\mathbf{k}+\mathbf{q}-\mathbf{Q},\alpha} \gamma^{v}_{\mathbf{k},\alpha}\rangle$$

$$= -2\sum_{\mathbf{k},\alpha} u_{\mathbf{k}+\mathbf{q}-\mathbf{Q}} v_{\mathbf{k}} \langle h_{\mathbf{k}+\mathbf{q}-\mathbf{Q},\alpha} h^{\dagger}_{\mathbf{k},\alpha}\rangle$$

$$= -2\,\delta_{\mathbf{q},\mathbf{Q}+\mathbf{K}} \sum_{\mathbf{k},\alpha} u_{\mathbf{k}+\mathbf{K}} v_{\mathbf{k}} \langle h_{\mathbf{k}+\mathbf{K},\alpha} h^{\dagger}_{\mathbf{k},\alpha}\rangle$$

$$-2\,\delta_{\mathbf{q},\mathbf{Q}+\mathbf{K}} \sum_{\mathbf{k},\alpha} u_{\mathbf{k}+\mathbf{K}} v_{\mathbf{k}} t_k w_k$$

$$\times (\langle d^{+}_{\mathbf{k},\alpha} d^{+\dagger}_{\mathbf{k},\alpha}\rangle - \langle d^{-}_{\mathbf{k},\alpha} d^{-\dagger}_{\mathbf{k},\alpha}\rangle), \tag{A30}$$

and one sees that the magnetization is now peaked around $\mathbf{Q}+\mathbf{K}$ instead of $\mathbf{Q}$. For stripes aligned along the **y** direction this is possible of course when

$$\mathbf{K} = \pm \frac{2\pi}{l}\mathbf{x}, \tag{A31}$$

where l is the interstripe distance.

APPENDIX B: DIPOLES OF THE *T-J* MODEL

Let us consider the SDW theory of the t-J model as proposed by Shraiman and Siggia,[30] described by

$$H = -t\sum_{\langle i,j\rangle} c^{\dagger}_{i,\sigma} c_{j,\sigma} + \text{H.c.} + J\sum_{\langle i,j\rangle} \mathbf{S}_i \cdot \mathbf{S}_j, \tag{B1}$$

and use the slave fermion representation

$$c_{i,\sigma} = \psi^{\dagger}_{\alpha,i} z_{\alpha,i,\sigma}, \tag{B2}$$

where $\psi^{\dagger}_{\alpha,i}$ creates a hole (fermion) on a site i in the sublattice $\alpha = A,B$ (which labels the ''spin'' of the hole) and $z_{\alpha,i,\sigma}$ is a Schwinger boson on the same sublattice (spin wave). In order to obtain the dynamics of the holes alone we trace out the spin-wave degrees of freedom. The static part of the interaction is[30]

$$H_{SS} = -\frac{1}{N}\sum_{\mathbf{k},\mathbf{k}',\mathbf{q}} V(\mathbf{k},\mathbf{k}',\mathbf{q})\,\psi^{\dagger}_{A}(\mathbf{k})\,\psi_{B}(\mathbf{k}+\mathbf{q})$$
$$\times \psi^{\dagger}_{B}(\mathbf{k}'+\mathbf{q})\,\psi_{A}(\mathbf{k}'), \tag{B3}$$

where the momentum sum is restricted to the magnetic Brillouin zone and

$$V(\mathbf{k},\mathbf{k}',\mathbf{q}) = -g\left[\frac{(\lambda_{\mathbf{k}}-\lambda_{\mathbf{k}+\mathbf{q}})(\lambda_{\mathbf{k}'}-\lambda_{\mathbf{k}'+\mathbf{q}})}{1-\lambda_{\mathbf{q}}} + \frac{(\lambda_{\mathbf{k}}+\lambda_{\mathbf{k}+\mathbf{q}})(\lambda_{\mathbf{k}'}+\lambda_{\mathbf{k}'+\mathbf{q}})}{1+\lambda_{\mathbf{q}}}\right], \tag{B4}$$

with

$$\lambda_{\mathbf{q}} = \frac{1}{2}[\cos(q_x)+\cos(q_y)]. \tag{B5}$$

The coupling constant g is a function of t and J. In the strong coupling limit ($t \ll J$) $g \approx 8t^2/J$, while in the weak coupling limit ($t \gg J$) we have $g \approx J$.[29]

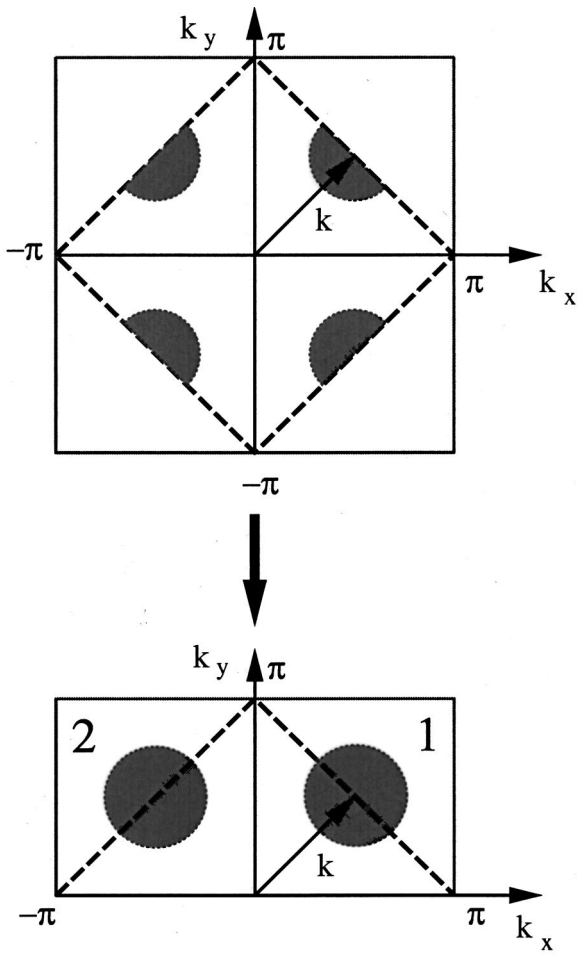

FIG. 15. Choice of the BZ.

Observe that Eq. (B3) does not have a kinetic term for the holes. The kinetic energy has to be obtained from the hole self-energy at zero frequency and can be written as

$$H_0 = \sum_{\mathbf{k},\alpha=A,B} \epsilon_{\mathbf{k}} \psi^{\dagger}_{\alpha}(\mathbf{k})\,\psi_{\alpha}(\mathbf{k}), \tag{B6}$$

where $\epsilon_{\mathbf{k}}$ has a minimum at $(\pm\pi/2,\pm\pi/2)$.[30] For a low density of holes these are the only points of interest and therefore we can look at the interaction (B4) strength close to these points. Observe that at these points we have $\lambda_{\mathbf{q}} \to 0$ and therefore the interactions are dominated by the first term in Eq. (B4) which describes the fluctuations of the staggered magnetization [with characteristic wave vector $\mathbf{Q}=(\pi,\pi)$]. The second term describes the fluctuations of the homogeneous magnetization ($\mathbf{q}=0$), which is not of direct interest here. In this case, for $\mathbf{k}$ and $\mathbf{k}'$ close ($\pm\pi/2,\pm\pi/2$) to the interaction can be approximated by

$$V(\mathbf{k},\mathbf{k}',\mathbf{q}) \approx -g\,\frac{\lambda_{\mathbf{k}+\mathbf{q}}\lambda_{\mathbf{k}'+\mathbf{q}}}{1-\lambda_{\mathbf{q}}}. \tag{B7}$$

The problem can be further simplified if one works with the upper half-part of the original BZ instead of the magnetic BZ, as shown in Fig. 15. This can be accomplished by a shift of the lower part of the BZ by **Q**.

Moreover, working in the long-wavelength limit, that is, with $\mathbf{q}\to 0$, one sees that there are four values of $V(\mathbf{k},\mathbf{k}',\mathbf{q})$ of relevance: (1) when $\mathbf{k}=\mathbf{k}'=\mathbf{Q}/2$,

$$V_{11}(\mathbf{q})\approx -g\frac{(q_x+q_y)^2}{q^2}; \tag{B8}$$

(2) when $\mathbf{k}=\mathbf{k}'=\mathbf{Q}^*/2$ [where $\mathbf{Q}^*=(-\pi,\pi)$] and

$$V_{22}(\mathbf{q})\approx -g\frac{(q_x-q_y)^2}{q^2}; \tag{B9}$$

(3) when $\mathbf{k}=\mathbf{Q}/2$ and $\mathbf{k}'=\mathbf{Q}^*/2$,

$$V_{12}(\mathbf{q})\approx g\frac{q_x^2-q_y^2}{q^2}; \tag{B10}$$

(4) and finally $\mathbf{k}=\mathbf{Q}^*/2$ and $\mathbf{k}'=\mathbf{Q}/2$,

$$V_{21}(\mathbf{q})=V_{12}(\mathbf{q}). \tag{B11}$$

We can now split the sums in Eq. (B3) to the regions around these two points and introduce a cutoff in the momentum sum Λ such that $q\ll\Lambda\ll\pi$. In this case the Hilbert space of the problem is divided into two different sub-Hilbert spaces and the hole operator can be rewritten as

$$\psi_{\alpha,i}=\sum_{\mathbf{k}} e^{i\mathbf{k}\cdot\mathbf{r}_i}\psi_\alpha(\mathbf{k})\approx\psi_{\alpha,i,1}\cos\left(\frac{\mathbf{Q}}{2}\cdot\mathbf{r}\right)+\psi_{\alpha,i,2}\cos\left(\frac{\mathbf{Q}^*}{2}\cdot\mathbf{r}\right), \tag{B12}$$

where

$$\psi_{\alpha,i,1}\approx\sum_{\mathbf{q}} e^{i\mathbf{q}\cdot\mathbf{r}_i}\psi_\alpha\left(\frac{\mathbf{Q}}{2}+\mathbf{q}\right),$$

$$\psi_{\alpha,i,2}\approx\sum_{\mathbf{q}} e^{i\mathbf{q}\cdot\mathbf{r}_i}\psi_\alpha\left(\frac{\mathbf{Q}^*}{2}+\mathbf{q}\right). \tag{B13}$$

It is convenient to define the operator

$$p_a(\mathbf{q})=\sum_{\mathbf{k}}\psi^\dagger_{B,a}(\mathbf{k}+\mathbf{q})\psi_{A,a}(\mathbf{k}),$$

$$p_a^\dagger(\mathbf{q})=\sum_{\mathbf{k}}\psi^\dagger_{A,a}(\mathbf{k})\psi_{B,a}(\mathbf{k}+\mathbf{q})=\sum_{\mathbf{k}}\psi^\dagger_{A,a}(\mathbf{k}-\mathbf{q})\psi_{B,a}(\mathbf{k}), \tag{B14}$$

with $a=1,2$. Using these new operators and results (B8)–(B11), we can rewrite the Hamiltonian (B3) as

$$\begin{aligned}H_{SS}\approx -\frac{g}{N}\sum_{\mathbf{q}}\frac{1}{q^2}\{&q^2[p_1^\dagger(\mathbf{q})p_1(\mathbf{q})+p_2^\dagger(\mathbf{q})p_2(\mathbf{q})]\\&-(q_x^2-q_y^2)[p_1^\dagger(\mathbf{q})p_2(\mathbf{q})+p_2^\dagger(\mathbf{q})p_1(\mathbf{q})]\\&+2q_xq_y[p_1^\dagger(\mathbf{q})p_1(\mathbf{q})-p_2^\dagger(\mathbf{q})p_2(\mathbf{q})]\}.\end{aligned} \tag{B15}$$

This does not have a very transparent form. In order to see that this Hamiltonian has the form of a dipole-dipole interaction we define the vector operator

$$\mathbf{D}(\mathbf{q})=\frac{1}{\sqrt{2}}(p_1(\mathbf{q})-p_2(\mathbf{q}),p_1(\mathbf{q})+p_2(\mathbf{q})),$$

$$\mathbf{D}^\dagger(\mathbf{q})=\frac{1}{\sqrt{2}}(p_1^\dagger(-\mathbf{q})-p_2^\dagger(-\mathbf{q}),p_1^\dagger(-\mathbf{q})+p_2^\dagger(-\mathbf{q})) \tag{B16}$$

and rewrite Eq. (B15) as

$$\begin{aligned}H_{SS}\approx -\frac{g}{N}\sum_{\mathbf{q}}\frac{1}{q^2}\Bigg[&q^2\mathbf{D}^\dagger(\mathbf{q})\cdot\mathbf{D}(\mathbf{q})+\mathbf{D}^\dagger(-\mathbf{q})\cdot\mathbf{D}(\mathbf{q})\\&-2\frac{[\mathbf{D}^\dagger(-\mathbf{q})\cdot\mathbf{q}][\mathbf{D}(\mathbf{q})\cdot\mathbf{q}]}{q^2}\Bigg].\end{aligned} \tag{B17}$$

Observe that the first term in Eq. (B17) is q-independent and will lead to a local interaction that has the usual scalar form. We are interested in the second part of the Hamiltonian. Defining the Fourier transform

$$D(\mathbf{r})=\sum_{\mathbf{q}} e^{i\mathbf{q}\cdot\mathbf{r}}D(\mathbf{q}), \tag{B18}$$

the second term in Eq. (B17) acquires the required form

$$\begin{aligned}H_{dd}=g\int d\mathbf{r}\int d\mathbf{r}'\frac{1}{(\mathbf{r}-\mathbf{r}')^2}\Bigg\{&\mathbf{D}^\dagger(\mathbf{r})\cdot\mathbf{D}(\mathbf{r}')\\&-2\frac{[\mathbf{D}^\dagger(\mathbf{r})\cdot\mathbf{r}][\mathbf{D}(\mathbf{r}')\cdot\mathbf{r}']}{(\mathbf{r}-\mathbf{r}')^2}\Bigg\},\end{aligned} \tag{B19}$$

which is the second quantized form of the magnetic dipole-dipole interaction.

In order to put this Hamiltonian in a form involving the magnetic dipole defined by Shraimann and Siggia consider their definition:[30]

$$P_{\mu,\alpha}(\mathbf{q})=\sum_{\mathbf{k},a,b}\sin(k_\alpha)\psi_a^\dagger(\mathbf{k}+\mathbf{q})\tau^\mu_{a,b}\psi_b(\mathbf{k}), \tag{B20}$$

where $\mu=x,y,z$ refers to indices of the Pauli matrices $\tau^\mu_{a,b}$ and therefore act in the sub-space of the sublattices A and B and $\alpha=x,y$ refers to the space indices. In particular, the lowering and raising operators associated with this magnetic dipole operators have the interesting form

$$P_{-,\alpha}(\mathbf{q})=2\sum_{\mathbf{k}}\sin(k_\alpha)\psi_B^\dagger(\mathbf{k}+\mathbf{q})\psi_A(\mathbf{k}),$$

$$P_{+,\alpha}(\mathbf{q})=2\sum_{\mathbf{k}}\sin(k_\alpha)\psi_A^\dagger(\mathbf{k}+\mathbf{q})\psi_B(\mathbf{k}). \tag{B21}$$

In the approximation we are employing we can split the summation in Eqs. (B21) around $\mathbf{Q}$ and $\mathbf{Q}^*$ in order to get (this can be done because the sine function is smooth around these two points)

$$P_{-,x}(\mathbf{q})\approx 2\sum_{\mathbf{k}}[\psi^\dagger_{B,1}(\mathbf{k}+\mathbf{q})\psi_{A,1}(\mathbf{k})-\psi^\dagger_{B,2}(\mathbf{k}+\mathbf{q})\psi_{A,2}(\mathbf{k})]$$

$$P_{-,y}(\mathbf{q}) \approx 2\sum_{\mathbf{k}} [\psi^{\dagger}_{B,1}(\mathbf{k}+\mathbf{q})\psi_{A,1}(\mathbf{k}) + \psi^{\dagger}_{B,2}(\mathbf{k}+\mathbf{q})\psi_{A,2}(\mathbf{k})]$$

$$P_{+,x}(\mathbf{q}) \approx 2\sum_{\mathbf{k}} [\psi^{\dagger}_{A,1}(\mathbf{k}+\mathbf{q})\psi_{B,1}(\mathbf{k}) - \psi^{\dagger}_{A,2}(\mathbf{k}+\mathbf{q})\psi_{B,2}(\mathbf{k})]$$

$$P_{+,y}(\mathbf{q}) \approx 2\sum_{\mathbf{k}} [\psi^{\dagger}_{A,1}(\mathbf{k}+\mathbf{q})\psi_{B,1}(\mathbf{k}) + \psi^{\dagger}_{A,2}(\mathbf{k}+\mathbf{q})\psi_{B,2}(\mathbf{k})], \tag{B22}$$

where the signs come from value of the sines around the two points at the Fermi surface. These dipole operators can be also written trivially in terms of the operators in Eqs. (B14):

$$P_{-,x}(\mathbf{q}) = 2[p_1(\mathbf{q}) - p_2(\mathbf{q})],$$

$$P_{-,y}(\mathbf{q}) = 2[p_1(\mathbf{q}) + p_2(\mathbf{q})], \tag{B23}$$

and so on. By direct comparison with Eqs. (B16) one finds

$$\mathbf{D}(\mathbf{q}) = \frac{1}{2\sqrt{2}}(P_{-,x}(\mathbf{q}), P_{-,y}(\mathbf{q})), \tag{B24}$$

which makes clear the connection. On taking the Fourier transform of the magnetic dipole operators back to real space one finds, for instance,

$$D_{x,i} = \frac{1}{\sqrt{2}}(\psi^{\dagger}_{B,1,i}\psi_{A,1,i} - \psi^{\dagger}_{B,2,i}\psi_{A,2,i}),$$

$$D_{y,i} = \frac{1}{\sqrt{2}}(\psi^{\dagger}_{B,1,i}\psi_{A,1,i} + \psi^{\dagger}_{B,2,i}\psi_{A,2,i}). \tag{B25}$$

This explicitly justifies our earlier claim that the dipolar interaction is due to the coherent hoping of holes between two different sublattices (at the same position in space).

*Also at the Institute of Semiconductor Physics, Novosibirsk, Russia.

[1] V.J. Emery, S.A. Kivelson, and O.V. Zachar, Phys. Rev. B **56**, 6120 (1997).

[2] Y. Yacoby, S.M. Held, and E.A. Stern, Solid State Commun. **101**, 801 (1997); A. Aharony and A. Auerbach, Phys. Rev. Lett. **70**, 1874 (1993), and references therein.

[3] *Phase Separation in Cuprate Superconductors*, edited by K. A. Müller and G. Benedek (World Scientific, Singapore, 1993).

[4] See, e.g., R.H. McKenzie, Phys. Rev. Lett. **74**, 5140 (1995), and references therein.

[5] See, e.g., J.P. Lorenzo and S. Aubry, Physica D **113**, 76 (1998), and references therein.

[6] See, e.g., S. Yunoki, A. Moreo,and E. Dagotto, Phys. Rev. Lett. **81**, 5612 (1998), and references therein.

[7] J.M. Tranquada, D.J. Buttrey, and D.E. Rice, Phys. Rev. Lett. **70**, 445 (1993).

[8] S. Mori, C.H. Chen, and S.W. Cheong, Nature (London) **392**, 473 (1998).

[9] J.M. Tranquada, B.J. Sternlieb, J.D. Axe, Y. Nakamura, and S. Uchida, Nature (London) **375**, 561 (1995).

[10] A. Bianconi, Phys. Rev. B **54**, 12018 (1996); M.V. Zimmermann, A. Vigliante, T. Niemoller, N. Ichikawa, T. Frello, J. Madsen, P. Wochner, S. Uchida, N.H. Andersen, and J.M. Tranquada, Europhys. Lett. **41**, 629 (1998).

[11] P.C. Canfield and J. D. Thompson, in *Phase Separation in Cuprate Superconductors*, edited by E. Sigmund and K. Alex Müller (Springer-Verlag, Berlin, 1994); B. W. Statt, P. C. Hammel, Z. Fisk, S-W. Cheong, F. C. Chou, and D. C. Johnston, and J. E. Schirber, Phys. Rev. B **52**, 15 575 (1995); N. J. Curro, P. C. Hammel, B. J. Suh, M. Hücker, B. Büchner, U. Ammerahl, and A. Revcolevschi, Phys. Rev. Lett. (to be published).

[12] J.H. Cho, F.C. Chou, and D.C. Johnson, Phys. Rev. Lett. **70**, 222 (1993).

[13] F.C. Chou, F. Borsa, J.H. Cho, D.C. Johnston, A. Lascialfari, D.R. Torgeson, and J. Ziolo, Phys. Rev. Lett. **71**, 2323 (1993).

[14] F. Borsa, P. Carretta, J.H. Cho, F.C. Chou, Q. Hu, D.C. Johnston, A. Lascialfari, D.R. Torgeson, R.J. Gooding, N.M. Salem, and K.J.E. Vos, Phys. Rev. B **52**, 7334 (1995).

[15] S. Wakimoto, G. Shirane, Y. Endoh, K. Hirota, S. Ueki, K. Yamada, R.J. Birgeneau, M.A. Kastner, Y.S. Lee, P.M. Gehring, and S.H. Lee, Phys. Rev. B **60**, R769 (1999).

[16] J.M. Tranquada, Physica C **282**, 166 (1997).

[17] G. Aeppli, T. Mason, S.M. Hayden, H.A. Mook, and J. Kulda, Science **278**, 1432 (1997).

[18] H.J. Schulz, J. Phys. (France) **50**, 2833 (1989); J. Zaanen, and J. Gunnarsson, Phys. Rev. B **40**, 7391 (1989); A.R. Bishop, F. Guinea, P.S. Lomdahl, E. Louis, and J.A. Verges, Europhys. Lett. **14**, 157 (1991).

[19] P. Prelovsek and X. Zotos, Phys. Rev. B **47**, 5984 (1993); P. Prelovsek and I. Sega, *ibid.* **49**, 15 241 (1994); E.W. Carlson, S.A. Kivelson, Z. Nussinov, and V.J. Emery, *ibid.* **57**, 14 704 (1998); C. Nayak and F. Wilczek, Phys. Rev. Lett. **78**, 2465 (1997); A.H. Castro Neto, Z. Phys. B: Condens. Matter **103**, 185 (1997); J. Zaanen, O.Y. Osman, and W. van Saarloos, Phys. Rev. B **58**, R11 868 (1998); M. Vojta and S. Sachdev, Phys. Rev. Lett. **83**, 3916 (1999).

[20] A.L. Chernyshev, A.H. Castro Neto, and A.R. Bishop, Phys. Rev. Lett. **84**, 4922 (2000).

[21] G. Seibold, C. Castellani, C. DiCastro, and M. Grilli, Phys. Rev. B **58**, 13506 (1998).

[22] V.J. Emery and S.A. Kivelson, Physica C **209**, 597 (1993).

[23] U. Löw, V.J. Emery, K. Fabricius, and S.A. Kivelson, Phys. Rev. Lett. **72**, 1918 (1994).

[24] F. Guinea, G. Gomez-Santos, and D. Arovas, cond-mat/9907184 (unpublished).

[25] S.R. White and D.J. Scalapino, Phys. Rev. Lett. **80**, 1272 (1998); **81**, 3227 (1998).

[26] C.S. Hellberg and E. Manousakis, Phys. Rev. Lett. **83**, 132 (1999); Phys. Rev. Lett. **84**, 3022 (2000); S.R. White and D.J. Scalapino, Phys. Rev. Lett. **84**, 3201 (2000).

[27] J. Zaanen (private communication).

[28] J.R. Schrieffer, X.G. Wen, and S.C. Zhang, Phys. Rev. B **39**, 11 663 (1989).

[29] D.M. Frenkel and W. Hanke, Phys. Rev. B **42**, 6711 (1990).

[30] B.I. Shraiman and E.D. Siggia, Phys. Rev. B **40**, 9162 (1989).

[31] S.A. Kivelson, E. Fradkin, and V.J. Emery, Nature (London) **393**, 550 (1998).

[32] J.C. Slater, Phys. Rev. **82**, 538 (1951).

[33] N. F. Mott, *Metal-Insulator Transitions* (Taylor and Francis, London, 1974), p. 141.

[34] B.O. Wells, Z.X. Shen, A. Matsuura, D.M. King, M.A. Kastner, M. Greven, and R.J. Birgenau, Phys. Rev. Lett. **74**, 964 (1995).
[35] A. Chubukov and K. Muselian, Phys. Rev. B **51**, 12 605 (1995).
[36] E. Fradkin, *Field Theories of Condensed Matter Systems* (Addison-Wesley, Redwood City, 1991), p. 48.
[37] S. Chakravarty, B.I. Halperin, and D.R. Nelson, Phys. Rev. Lett. **60**, 1057 (1988).
[38] We are thankful to S. Kivelson for attracting our attention to this problem.
[39] A. Aharony, R.J. Birgenau, A. Coniglio, M.A. Kastner, and H.E. Stanley, Phys. Rev. Lett. **60**, 1330 (1988).
[40] N. Grønbech-Jensen, G. Hummer, and K.M. Beardmore, Mol. Phys. **92**, 941 (1997).
[41] J. Lekner, Physica A **176A**, 485 (1991).
[42] J. Bonča and J.E. Gubernatis, Phys. Rev. E **53**, 6504 (1996).
[43] W.H. Press, S.A. Teukolsky, W.T. Vetterling, and B.P. Flannery, *Numerical Recipes: The Art of Scientific Computing* (Cambridge University Press, Cambridge, 1992).
[44] E.P. Wigner, Phys. Rev. **46**, 1002 (1934).
[45] N.M. Salem and R.J. Gooding, Europhys. Lett. **35**, 603 (1996).
[46] P.W. Anderson, *Basic Notions in Condensed Matter* (Addison-Wesley, Reading, 1997).
[47] B.P. Stojkovic, Z.G. Yu, A.R. Bishop, A.H. Castro Neto, and Niels Grønbech-Jensen, Phys. Rev. Lett. **82**, 4679 (1999).
[48] This is a highly degenerate configuration which can be mapped into a classical six-vertex model. See, for instance, R. J. Baxter, *Exactly Solved Models in Statistical Mechanics* (Academic Press, London, 1982), p. 127.
[49] The simulations show the presence of topological defects in the phase of the magnetic dipole moments, i.e., the total phase in a loop may be shifted by 2π.
[50] Some impurities, on donating a hole or an electron to CuO planes, become charged ions.
[51] S. Zagoulaev, P. Monod, and J. Jegoudez, Phys. Rev. B **52**, 10474 (1995).
[52] R.J. Gooding, N.M. Salem, R.J. Birgeneau, and F.C. Chou, Phys. Rev. B **55**, 6360 (1997).
[53] J. Bardeen, Phys. Rev. Lett. **45**, 1978 (1980); D.S. Fisher, Phys. Rev. B **31**, 1396 (1985).
[54] See, e.g., M.B. Weissman, Physica D **107**, 421 (1997).
[55] See, e.g., C. Dasgupta, and O.T. Valls, Phys. Rev. E **59**, 3123 (1999).